Available online at www.sciencedirect.com
ScienceDirect
Journal of the European Ceramic Society 30 (2010) 2419–2426
www.elsevier.com/locate/jeurceramsoc

Analysis of the indentation size effect in brittle materials from nanoindentation load–displacement curve

T. Ebisu *, S. Horibe

Department of Modern Mechanical Engineering, Waseda University, 3-4-1 Ohkubo, Shinjuku-ku, Tokyo 169-8555, Japan

Received 6 December 2009; received in revised form 27 April 2010; accepted 11 May 2010
Available online 12 June 2010

Abstract

In this paper, we investigated the relationships between crack initiation/propagation, stress induced transformation and indentation size effect (ISE) using Universal hardness. Preparing three kinds of specimens, 8 mol%Y_2O_3–ZrO_2 single crystal (single 8Y-FSZ), 12 mol%CeO_2–ZrO_2 polycrystals (12Ce-TZP) and fused quartz, we were able to research the above relationships separately. The load dependence of universal hardness in the three specimens was studied using nanoindentation equipment and found that single 8Y-FSZ and 12Ce-TZP showed the ISE. To reveal the origin of the ISE in these materials, we analyzed the relationship between load–displacement curve and Universal hardness ISE. Adapting the second-order differential (d^2P/dh^2) to the load–displacement curve showed that a small displacement change (micro multiple pop-ins) would occur in each deformation process of the single 8Y-FSZ and 12Ce-TZP. The origin of the micro multiple pop-ins is considered to be crack initiation/propagation in single 8Y-FSZ and stress induced transformation in 12Ce-TZP, respectively, and these micro multiple pop-ins should result in the Universal hardness ISE.

Keywords: Hardness; Surface; ZrO_2; Nano-indentation

1. Introduction

Indentation hardness testing has been used for a long time to evaluate the mechanical properties of materials. This convenient testing method is popular among many kinds of researchers. Representative hardness tests include the Brinell test and the Vickers test. As for primary research use, the relationship between yield stress and indentation hardness of metals[1] and the hardness change caused by work-hardening[2] are reported. Following the above studies, the measurement of the brittle material's toughness using Vickers indentation method[3,4], measurement of elastic modulus-to-hardness with a Knoop indenter[5], relationship between stress induced transformation and hardness, impression geometry and transformation volume[6–8] were studied in detail. Since the development of industry these days is so rapid, it is necessary to measure the mechanical properties of thin film, fibers, and micro materials. To evaluate the hardness of materials, the conventional method is needed to get an impression. However, for materials like thin films, making impression large enough to be captured by optical microscopy with a high degree of accuracy is very difficult, and it is needed to use time-consuming electron microscopy to capture the images. As for methods which satisfy the above needs, the recently developed depth sensing indentation or dynamic indentation method (called nanoindentation method), is gathering interest as tools which can evaluate the mechanical properties of thin film surfaces and small materials.

The invention of the nanoindentation method has enabled us to measure the material properties from the macro- to nanoscale range. At this scale, a very interesting phenomenon occurs, the hardness increases as the indentation depth decreases.[9–14] This is named the indentation size effect (ISE). The shallower the depth is, the steeper the inclination of the hardness. It is said that ISE is caused by many factors. Li and Bradt[9] studied the microhardness ISE on the Knoop microhardness of single crystals of TiO_2 and SnO_2 and proposed that the ISE was a consequence of the indentation size proportional resistance of the test specimens (PSR) and consisted of the elastic resistance of the specimen and the frictional effects. Quinn and Quinn[10] reported that Vickers

* Corresponding author. Present address: Kobe Steel, LTD, Surface Technology Research Section, 15 Kinugaoka, Moka-city, Tochigi 321-4346, Japan.
E-mail address: ebisu.tomohiro@gmail.com (T. Ebisu).

0955-2219/$ – see front matter © 2010 Elsevier Ltd. All rights reserved.
doi:10.1016/j.jeurceramsoc.2010.05.006

hardness–load curves for a number of brittle ceramics exhibited a distinct transition to a plateau constant hardness level that corresponded well to a relationship between hardness, Young's modulus and fracture toughness. Nix and Gao[11] reported that the model of geometrically necessary dislocation provides an excellent description of the depth dependence of hardness of Cu and Ag in the micrometer depth regime and stated that hardness of a material should not depend strongly on the depth of indentation if the material was intrinsically hard. Quinn et al.[12] studied the Knoop hardness of some glasses and reported that cracked indentations were longer than uncracked indentations and the apparent hardness was consequently lower. Manika and Maniks[13] studied the ISE in single crystals, polycrystals and amorphous of solids and mentioned that both the surface effect and strain gradient effect were suggested to contribute to the ISE. Sahin et al.[14] reported that the load dependence of indentation hardness showed a typical ISE behavior in SiAlON–ZrO_2 ceramics which showed stress induced transformation.

The studies analyzing ISE from the continual surface change of deformation behavior have not so far been performed sufficiently. In this paper, we approached the relationships among ISE of crack initiation, stress induced transformation and load–displacement curve, which is the continual surface deformation changes data, obtained by nanoindentation equipment. As a specimen, the ceramics which showed less hardness change due to indentation depth and were less sensitive to environmental changes than metals in an air conditioned room were chosen. Fully stabilized zirconia ceramics which have low toughness and show no transformation induced by stress were used for analyzing the effects of cracks, and tetragonal zirconia polycrystals which have a very high toughness ratio and show stress induced transformation behavior were used for analyzing the transformation effect. To compare these two effects, we used fused quartz which shows no transformation and no crack initiation in low load indentation tests equipped with Berkovich indenter.

2. Experiment

2.1. Materials

8 mol%Y_2O_3 fully stabilized zirconia single crystal (single 8Y-FSZ), 12 mol%CeO_2 stabilized tetragonal zirconia polycrystals (12Ce-TZP) and fused quartz were used in this study. All specimens were rectangular in shape with parallel surfaces. Nanoindentation was conducted after making all specimen surfaces mirror finished. The reason we used single crystals for 8Y-FSZ and polycrystals for 12Ce-TZP was that the hardness of cubic zirconia crystal is largely dependent on the crystal orientation largely but that of zirconia tetragonal crystal is not.[8] Here, on single 8Y-FSZ, nanoindentation was carried out on (1 1 0) surface but we did not take the orientation effect into consideration in this study.

Nanoindentation experiments were performed using a dynamic ultramicrohardness tester instrument (DUH-W201, Shimadzu Corporation, Kyoto, Japan), with a displacement resolution of 1 nm and a force resolution of 0.2 μN. A diamond Berkovich indenter was used. In all tests, the maximum load was set as 1900 mN. Loading–unloading velocity of 70.6 mN/s was selected with a holding period duration of 10 s at the maximum load of 1900 mN. Tests were performed 8 times per specimen and the average value was calculated. The error bars represent the standard deviation obtained from the eight measurements of each specimen.

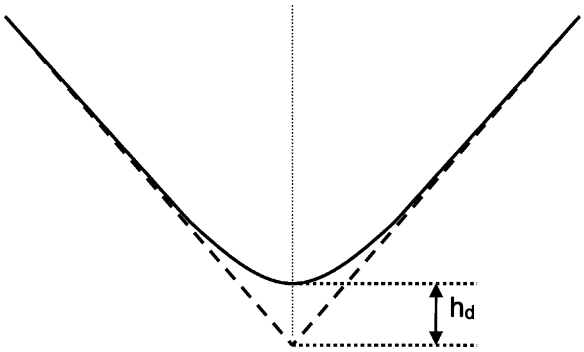

Fig. 1. Schematic diagram of the indenter with a tip rounding.

Oliver and Pharr[15] reported that load frame compliance C_f could be a significant fraction of the total displacement and tip rounding h_d could lead the area function for a perfect Berkovich indenter to deviate from Berkovich geometry. To clarify the true displacement of the indenter, we calculated C_f and h_d (the schematic figure of h_d is shown in Fig. 1) according to the correction method of Sun et al.[16]

$$h_{\text{total}} = C_f \cdot P + K^{-1/2} \cdot P^{1/2} - h_d \tag{1}$$

where P is the load, K is a constant and h_{total} is the displacement which the nanoindentation machine put out (no correction is carried out). Adapting Eq. (1) for the load–displacement curve of fused quartz in the load range of 200–1900mN, we obtained C_f and h_d values as follows, $C_f = 0.223 \pm 0.024$ nm/mN, $h_d = 100.2 \pm 5.9$ nm. The load–displacement curve of the fused quartz in this load range after being corrected with C_f and h_d showed $P \propto h^{1.96}$ implying that Eq. (1) is a good polynomial as the fitting function. Displacement h_{th} originating from the thermal effect was corrected assuming that displacement caused by thermal drift rate was constant throughout the test. The displacement h from the next paragraph is the corrected value with respect to C_f and h_{th}. The h_d value was not corrected but was used in each equation.

The elastic modulus was calculated following Eqs. (2)–(5). Projected contact area A_c of the ideal geometry indenter is expressed as follows:

$$A_c = 23.97(h_c + h_d)^2 \tag{2}$$

where h_c is the contact depth immediately before unloading and h_d is the tip rounding. h_c is given by

$$h_c = h - \varepsilon \frac{P}{S} \tag{3}$$

where h is displacement just before unloading and ε is the geometric constant and the value $\varepsilon = 0.75$ is generally used. P is the maximum load and S is the stiffness of the upper portion of the unloading data (assuming the data of 100–70% load range is

Table 1
Elastic modulus and Poisson's ratio in single 8Y-FSZ, 12Ce-TZP and fused quartz.

Material	Elastic modulus (GPa) (present experiment)	Elastic modulus (GPa) (literature)	Poisson's ratio
Single 8Y-FSZ (1 1 0)	215 ± 4.3	257.2[17]	0.25[17]
12Ce-TZP	167 ± 4.4	195[18]	0.31[18]
Fused quartz	75.3 ± 0.4	72[15]	0.17[19]

linear). Next, the reduced modulus is calculated following Eqs. (4) and (5).

$$E_r = \frac{S}{2} \cdot \sqrt{\frac{\pi}{A_c}} \tag{4}$$

$$\frac{1}{E_r} = \frac{(1-\nu^2)}{E} + \frac{(1-\nu_i^2)}{E_i} \tag{5}$$

where ν_i and ν are Poisson's ratio of the diamond and the specimen, E_i and E are Young's modulus of them. The parameters of ν_i and E_i were chosen as 0.07 and 1140 GPa. Poisson's ratio of the three specimens was referred from literature values and is listed in Table 1.[15,17–19]

The hardness parameter used in this study was the universal hardness (HU) measured from the indenter penetration depth.[20] HU is given by

$$HU = 37.838 \cdot \frac{P}{(h+h_d)^2} \tag{6}$$

where P is the load (mN) and h is the displacement (μm) of the loading cycle. Since the universal hardness was calculated from the surface area of the diamond that plunges beneath the original surface of the indented plane, it had both elastic and plastic components.

The surface images of the specimens was observed by SEM to clarify whether crack initiation occurred or not, and to assess the impression shape accurately. The presence of the monoclinic phase resulted from indentation induced transformation was detected using micro-Raman spectroscopy instrument (NRS-2000, JASCO Corporation, Tokyo, Japan) equipped with an Ar ion laser (532 nm wavelength). We investigated two points of 12Ce-TZP, one was the center of the impression and the other was a point far from the impression (over 40 μm from impression). We also investigated Ce-TZP stabilized in the monoclinic phase to compare with the tetragonal phase.

3. Results

3.1. Load–displacement curve, SEM and Elastic modulus

Fig. 2(a) shows the load–displacement (P–h) curve for single 8Y-FSZ. The curve demonstrates a smooth shape and no pop-ins could be detected. Fig. 2(b) shows the SEM image of single 8Y-FSZ impression. Well-defined cracks emerge from three sides of the corner. Figs. 3(a) and 4(a) are the P–h curves of 12Ce-TZP and fused quartz. Both curves show smooth shapes and no pop-in behavior. Figs. 3(b) and 4(b) are the SEM images

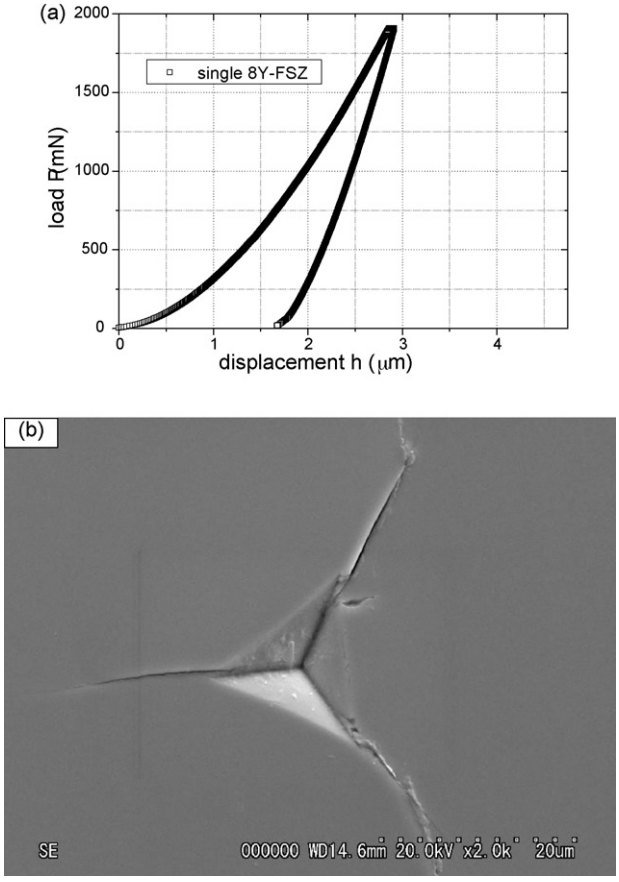

Fig. 2. Load–displacement data for single 8Y-FSZ obtained during nanoindentation with Berkovich indenter showing no sign of pop-in (a). And the SEM image of the impression at an applied load of 1900 mN (b).

of 12Ce-TZP and fused quartz. Both images show no trace of cracks. Characteristics in common with these three specimens are that they all exhibit sink-in at the edge of impressions.

Elastic modulus obtained in present work, elastic modulus from literature and Poisson's ratio on each specimen are listed in Table 1. Elastic modulus of single 8Y-FSZ shows a smaller value (−16%) than that from the literature.[17] It is important to confirm that the cubic zirconia Ref. 17 used was 10 mol% Y_2O_3 and Young modulus was calculated at a low load range (P_{max} = 1 mN). Since no nanoindentation data could be detected for Ce-TZP, we referred to the flexural resonant vibration test results in Ref. 18. Clearly, the elastic modulus from nanoindentation was lower than that of Ref. 18 (−14%). The modulus of fused quartz, which exhibited no crack initiation and no transformation behavior, was very close to that of Ref. 19.

3.2. Universal hardness and Raman spectrum

The HU changes due to load increase are exhibited in Fig. 5. It is evident that all specimens showed their maximum HU around the load of 10 mN. Comparing the HU of the three specimens, we found that in the load range of $P \geq 200$ mN, the HU in fused quartz showed almost a constant value. On the other hand, the HU in single 8Y-FSZ and 12Ce-TZP decreased gradually as the load increased.

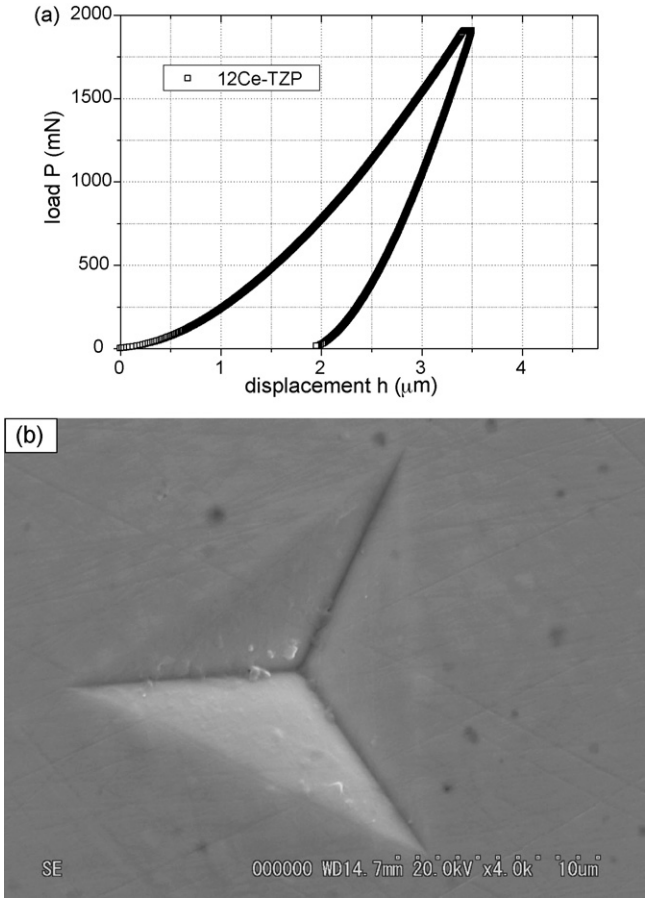

Fig. 3. Load–displacement data for 12Ce-TZP obtained during nanoindentation with Berkovich indenter showing no sign of pop-in (a). And the SEM image of the impression at an applied load of 1900 mN (b).

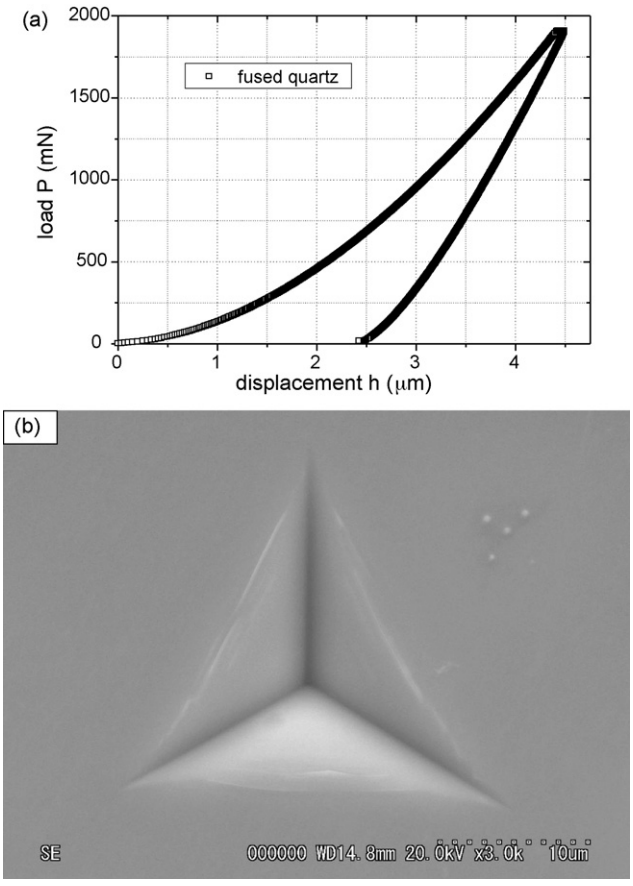

Fig. 4. Load–displacement data for fused quartz obtained during nanoindentation with Berkovich indenter showing no sign of pop-in (a). And the SEM image of the impression at an applied load of 1900 mN (b).

Fig. 6 is the Raman spectrums of the pre-indented surfaces (a), the center of the impression (b), and Ce-TZP stabilized in the monoclinic phase (c). (a) shows only the tetragonal phase and (c) exhibits only the monoclinic phase. However, the Raman spectrum of (b) shows both the tetragonal phase and monoclinic phase. This implies an occurrence of indentation induced transformation in 12Ce-TZP.

4. Analysis

The decrease in universal hardness in single 8Y-FSZ and 12Ce-TZP means that these materials exhibit ISE in universal hardness. However, the factors which caused the ISE in these specimens are not clear; we tried to approach this problem adapting the Meyer's law into *P–h* curve of the three specimens, and then discussed the each factor based on the material's characteristics.

4.1. Analysis method of ISE from P–h curve

According to Meyer's law, if the indenter has ideal geometry, load–diagonal length curve could be given by

$$P = C \cdot d^n \tag{7}$$

where P is the load, d is the diagonal length of impression, C is the material/indenter constant and n is the Meyer index due to the curvature of the curve. Since d is proportional to contact depth h_c and h_c are proportional to indentation depth h[21], So Eq. (7) could be expressed as follows:

$$P = C' \cdot h^n \tag{8}$$

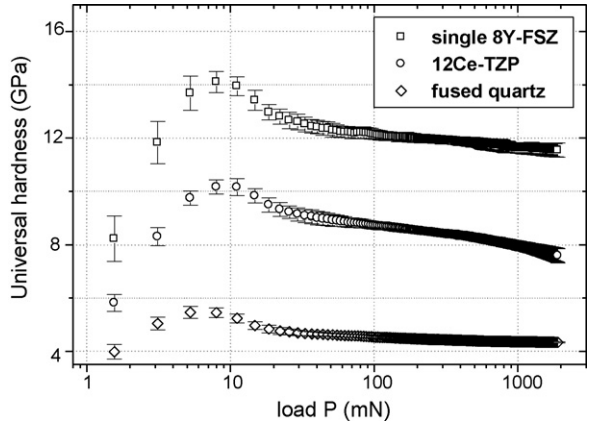

Fig. 5. Universal hardness as a function of the load in single 8Y-FSZ, 12Ce-TZP and fused quartz.

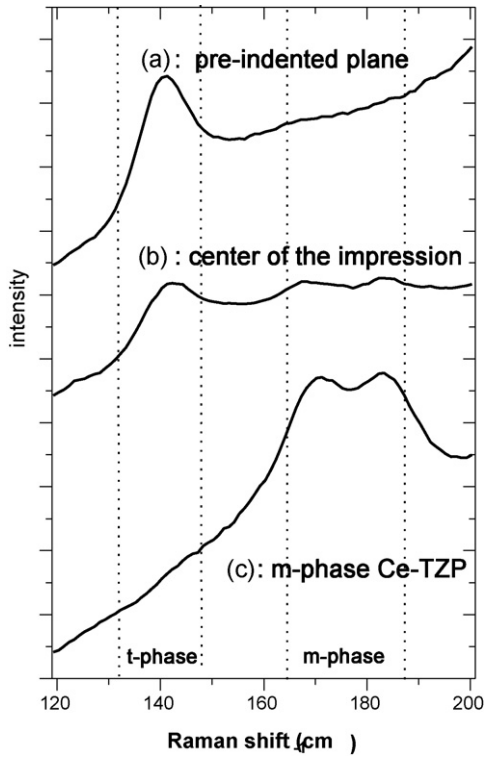

Fig. 6. Comparison of Raman spectrum in12Ce-TZP taken from the pre-indented plane (a), the center of the Berkovich indentation impression (b) and the plane stabilized in monoclinic phase (c).

where C' is constant. The important thing to distinguish in Eq. (8) is that the variable of the right term is not the contact depth h_c, but the indentation depth h. Fischer-Cripps[22] mentioned that if the plastic zone was fully developed (beyond elastic–plastic transition point), the load–displacement (P–h) curve of the loading section could be related to the square of the displacement ($P = C'h^2$). As for the loading stage of the P–h curve in the elastic–plastic field, Sakai[23] also stated that load is proportional to the square of the indentation depth. It is also important to assume that the P–h range Fischer and Sakai mentioned showed no pop-in behavior caused by crack initiation and less stress induced transformation behavior. If $n = 2$ in Eq. (7), the materials showed no ISE. If $n < 2$, the materials showed ISE and this case was confirmed by many materials.[24,25] The same phenomenon as in Eq. (7) could apply to Eq. (8) and $n = 2$ is just a form that Fischer-Cripps[22] and Sakai[23] mentioned. Taking the above fact into consideration, we analyzed the relationship between the P–h curve and ISE behavior in our experiment by differentiating the P–h curve of the three specimens.

The second-order differential against indentation depth h in Eq. (8) was provided for in the following equation:

$$\frac{d^2P}{dh^2} = n(n-1)\cdot C'\cdot h^{n-2} \tag{9}$$

Supposing that $n = 2$, d^2P/dh^2 in Eq. (9) is constant, and in the case $n < 2$, d^2P/dh^2 vs h exhibit the tendency that as h increases, d^2P/dh^2 decreases.

The above method, second-order differential of the P–h curve, was applied to the experimental P–h curve data. Here, to compare each datum easily, displacement h was normalized by maximum indentation depth h_{max} in each specimen and the data of the primary indentation depth at which tip rounding had a great influence on the deformation process was omitted. In particular, an indentation depth lower than $5 \times h_d$ (≒500 nm) data was omitted and converting this value in h/h_{max} put out $h/h_{max} \sim 0.15$ for single 8Y-FSZ, $h/h_{max} \sim 0.10$ for 12Ce-TZP and $h/h_{max} \sim 0.05$ for fused quartz.

4.2. d^2P/dh^2 vs h/h_{max} of three specimens

The index n was calculated from the P–h curve of single 8Y-FSZ in the load range of 200–1900mN, and the result that $n = 1.873$ means single 8Y-FSZ shows ISE behavior. This ISE result agrees well with the experimental results of another report[8] in which the hardness decreased as the indentation increased between the load range of 100–2000mN. Second-order differential (d^2P/dh^2) of the P–h curve in single 8Y-FSZ is shown in Fig. 7(a). Fig. 7(a) exhibits that d^2P/dh^2 decreases as indentation depth increases. This is also the same tendency of $n < 2$ in Eq. (9).

The same procedure as single 8Y-FSZ was conducted in the 12Ce-TZP P–h curve. Index $n = 1.808$ calculated from the P–h curve in the load range of 200–1900 mN agreed with the result that zirconia ceramics, which show stress induced transformation, have ISE behavior.[8,14] The second-order differential of the P–h curve in 12Ce-TZP is shown in Fig. 7(b), and this figure exhibits that as the indentation depth increases, d^2P/dh^2 decreases. This results would be equal to the tendency of $n < 2$ in Eq. (9).

Index $n = 1.961$ calculated from the P–h curve in the load range of 200–1900 mN in fused quartz means that this material shows next to no ISE behavior. Oliver and Pharr[15] also reported that quartz showed very little indentation size effect. The second-order differential of the P–h curve in fused quartz is exhibited in Fig. 7(c), and the d^2P/dh^2 maintains almost a constant value even given the depth change. This tendency corresponds to the case of $n = 2$ in Eq. (9).

5. Discussion

5.1. The origin of ISE in single 8Y-FSZ and 12Ce-TZP

From the above analysis results (Fig. 7) and experimental results (Fig. 5), the decrease in d^2P/dh^2 vs h is related to the Universal Hardness ISE (HU ISE) since the specimens which showed HU ISE behavior also had the tendency of decreasing in d^2P/dh^2 vs h. In the following paragraphs, we discuss the origin of the decrease in d^2P/dh^2 vs h, and then show the relationship between the HU ISE and the decrease in d^2P/dh^2 vs h in the schematic figures.

First, we discussed the crack initiation/propagation factor (single 8Y-FSZ). Preceding our study, Morris et al.[26] reported that crack pop-in was observed during loading for fused quartz and soda-lime glass, and stated that between one and four pop-in events have been detected during one indentation cycle. It should be reminded that crack pop-in should lead the d^2P/dh^2 vs h to

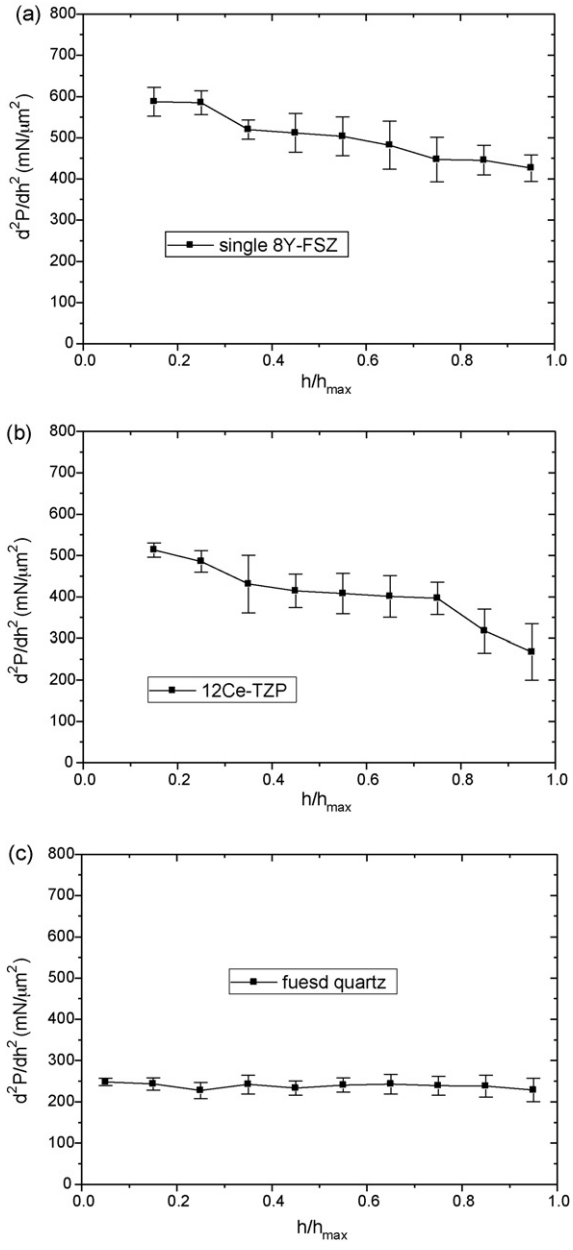

Fig. 7. Second-order differential (d^2P/dh^2) vs h/h_{max} of load–displacement curve in single 8Y-FSZ (a), 12Ce-TZP (b) and fused quartz (c).

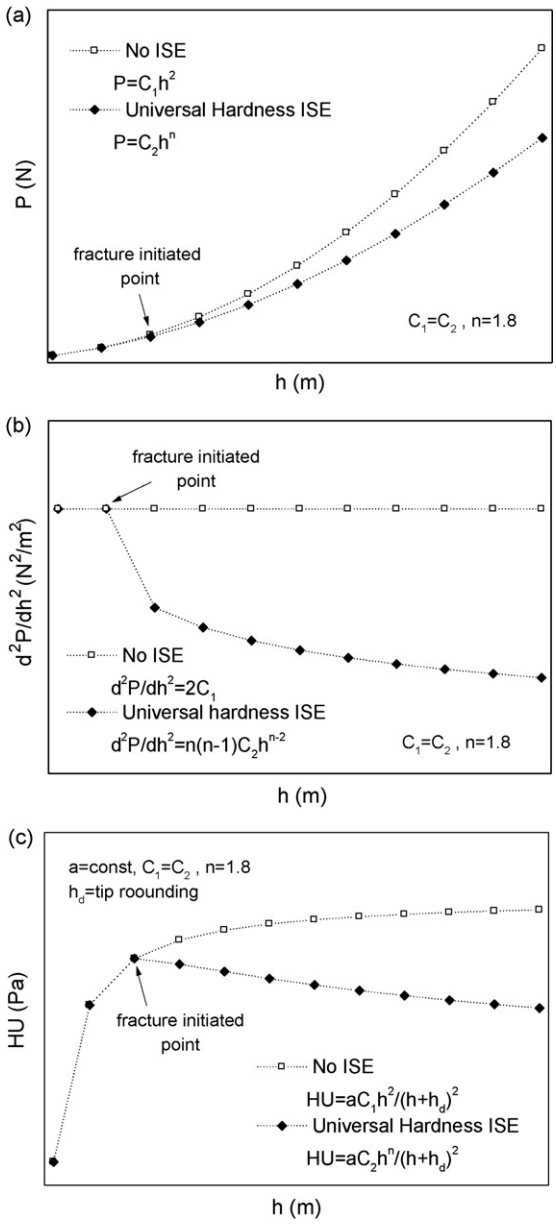

Fig. 8. Schematic no ISE and Universal hardness (HU) ISE figures of load–displacement curves (a), d^2P/dh^2 vs displacement (b) and HU vs displacement (c).

be deviated from the constant value since the d^2P/dh^2 should be equal to zero within the pop-in region. Field et al.[27] reported that following pop-in, the rate of penetration of the indenter increased. The rate of penetration after the pop-in should also have changed the trend of d^2P/dh^2 vs h. Quinn et al.[12] reported that cracking can significantly alter the hardness-load trends. Considering these reports, we suppose that the decrease in d^2P/dh^2 originates from a continuous small displacement jumps (we refer to these as micro multiple pop-ins), which are difficult to detect from a P–h curve, as used in our study, and that this micro multiple pop-ins would be caused by crack initiation/propagation in single 8Y-FSZ.

Next, we discussed the stress induced transformation factor (12Ce-TZP). Hannink and Swain[28] reported that there was an autocatalytic nucleation process of the transformation proceeding away from the contact site with a strong coupling to the shear stress trajectories and shear components of the transformation. Basu[29] reported that the presence of microcracks lead to a reduction in stiffness. We deduce that the reduction in stiffness caused by the microcracks due to transformation led to a decrease in the mean contact pressure as the load increased, and this would result in the occurrence of micro multiple pop-ins which should cause the decreases in d^2P/dh^2 in 12Ce-TZP.

Based on the theoretical equations, that are Eqs. (6), (8), and (9), Fig. 8 shows the schematic figures of the P–h curve (a), d^2P/dh^2 vs h (b) and HU vs h (c) in the case of no ISE

or HU ISE. Here, the HU ISE equations expressed in Fig. 8 are adopted after the fracture initiation (that is crack initiation/propagation and transformation in this paper), assuming that the transition of the surface behavior from "before fracture initiation" to "after fracture initiation" would be smooth. As for the n value in HU ISE, we gave the case of $n = 1.8$ considering the results of single 8Y-FSZ ($n = 1.873$) and 12Ce-TZP($n = 1.808$). It is evident that with or without a fracture, both P–h curves show the smooth shape. However, after the fracture initiation (HU ISE), the trends of d^2P/dh^2 vs h and HU vs h differed greatly from that of from no fracture initiation (no ISE). These schematic figures based on theoretical equations agree well with the experimental and analytical results in our study (Figs. 2–5 and 7).

From the above discussion, we consider that the HU ISE is related to the decrease in d^2P/dh^2 vs h, that is the micro multiple pop-ins which would be caused by crack initiation/propagation in single 8Y-FSZ and stress induced transformation in 12Ce-TZP.

However, we should state that further work would be needed to clarify the presence of micro multiple pop-ins which originate from crack initiation/propagation and stress induced transformation since we could not capture the continual deformation changes of the surface images.

5.2. The probability of ISE from other factors

5.2.1. Multiple pop-ins induced by the factors related to plastic deformation

Here, to clarify the origin of micro multiple pop-ins in our study, we should consider the slip effect which also causes multiple pop-ins. Multiple pop-ins caused by slip has been reported in the study of hexagonal crystals such as sapphire[30], GaN[31] and ZnO.[32] Nowak et al.[30] stated that step-ins (multiple pop-in) in the loading cycle of the hysteresis loops are due to rhombohedral twinning activated under a penetrating indenter. Kucheyev et al.[32] stated that materials where multiple pop-in events occur, have a hexagonal lattice structure, while semiconductors with a cubic structure exhibit the behavior of a single pop-in event upon loading. As for 12Ce-TZP, Hannink and Swain[28] reported that in all the TEM observations no evidence of dislocations were found, even in the extensively deformed regions about the indentation sites of 12Ce-TZP alloys. Considering the above studies, we deduced that micro multiple pop-ins in our study resulted from crack initiation/propagation in single 8Y-FSZ and stress induced transformation in 12Ce-TZP.

5.2.2. Effect of sink-in on hardness

McElhaney et al.[33] reported that the measured indentation hardnesses would be too high in the case of pile-ups and too low in the case of sink-in. In our study, all materials showed sink-in at the edge of the impression. We must notice that our hardness values were calculated from indentation depth and d^2P/dh^2 in fused quartz showed a constant value, which means that a material whose universal hardness does not change shows sink-in. The relationship between sink-in and the decrease in universal hardness could not be clarified in our study. Further studies are needed to clarify this effect.

Also, we would like to state that the hardness used in this study was universal hardness which differs from the conventional contact (impression) hardness. Therefore some different points might exist between these two hardness values since the factors like elastic recovery and crack closure are not taken into consideration in universal hardness. However, to understand the surface deformation changes correctly, universal hardness estimation is of great importance and gives us valuable information.

6. Conclusion

Preparing three types of specimens, single 8Y-FSZ (crack initiation/propagation), 12Ce-TZP (stress induced transformation) and fused quartz (none of them), and analyzing nanoindentation load–displacement curve in detail, we found the following results in this study.

1. Presence of indentation size effect (ISE) in Universal hardness (HU) in single 8Y-FSZ and 12Ce-TZP.
2. Effective analysis method for analyzing the ISE behavior from the nanoindentation load–displacement (P–h) curve (that is the second-order differential of load–displacement curve).
3. Presence of micro multiple pop-ins in the P–h curve, which might originate from crack initiation/propagation in single 8Y-FSZ and stress induced transformation in 12Ce-TZP, would cause the ISE in HU.

The important point in this paper is that all analyses were performed based not on contact hardness, but indentation depth (displacement). And further work would be needed to confirm the relationships among micro multiple pop-ins, crack initiation/propagation and stress induced transformation effects.

Acknowledgements

The authors would like to thank Prof. H. Kawada and his laboratory staffs Waseda University for their support in obtaining the measurements of the Raman spectrum. This research was supported by Waseda University Grant for Special Research Project (2008B-146).

References

1. Tabor D. The hardness of solids. *Rev Phys Technol* 1970;**1**:145.
2. Atkins AG, Tabor D. Plastic indentation in metals with cones. *J Mech Phys Solids* 1965;**13**:149.
3. Anstis GR, Chantikul P, Lawn BR, Marshall DB. A critical evaluation of indentation techniques for measuring fracture toughness: 1. Direct crack measurement. *J Am Ceram Soc* 1981;**64**:533.
4. Erbrahimi F, Kalwani L. Fracture anisotropy in silicon single crystal. *Mater Sci Eng A* 1999;**268**:116.
5. Marshall DB, Noma T, Evans AG. A simple method for determining elastic-modulus-to-hardness ratios using Knoop indentation measurements. *J Am Ceram Soc* 1982;**65**:C-175.

6. Tsukuma K, Shimada M. Strength, fracture toughness and Vickers hardness of CeO_2-stabilized tetragonal ZrO_2 polycrystals (Ce-TZP). *J Mater Sci* 1985;**20**:1178.
7. Reece MJ, Tetlow PL, Galiotis C. Phase transformation around indentations in zirconia. *J Mater Sci Lett* 1992;**11**:575.
8. Gogotsi GA, Dub SN, Lomonova EE, Ozersky BI. Vickers and Knoop indentation behavior of cubic and partially stabilized zirconia crystals. *J Eur Ceram Soc* 1995;**15**:405.
9. Li H, Bradt RC. The microhardness indentation load/size effect in rutile and cassiterite single crystals. *J Mater Sci* 1993;**28**:917.
10. Quinn JB, Quinn GD. Indentation brittleness of ceramics: a fresh approach. *J Mater Sci* 1997;**32**:4331.
11. Nix WD, Gao H. Indentation size effects in crystalline materials: a law for strain gradient plasticity. *J Mech Phys Solids* 1998;**46**:411.
12. Quinn GD, Green P, Xu K. Cracking and indentation size effect for Knoop hardness of glass. *J Am Ceram Soc* 2003;**86**:441.
13. Manika I, Maniks J. Size effects in micro- and nanoscale indentation. *Acta Mater* 2006;**54**:2049.
14. Sahin O, Uzun O, Sopicka-Lizer M, Gocmez H, Kolemen U. Analysis of load-penetration depth data using Oliver–Pharr and Cheng–Cheng methods of SiAlON–ZrO_2 ceramics. *J Phys D Appl Phys* 2008;**41**:35305.
15. Oliver WC, Pharr GM. An improved technique for determining hardness and elastic modulus using load and displacement sensing indentation experiments. *J Mater Res* 1992;**7**:1564.
16. Sun Y, Zheng S, Bell T, Smith J. Indenter tip radius and load frame compliance calibration using nanoindentation loading curves. *Phil Mag Lett* 1999;**79**:649.
17. Fujikane M, Setoyama D, Nagao S, Nowak R, Yamanaka S. Nanoindentation examination of yttria-stabilised zirconia (YSZ) crystal. *J Alloys Compd* 2007;**431**:250.
18. Kubota Y, Ashizuka M, Hokazono H. Elastic modulus and fracture toughness of CeO_2-containing tetragonal zirconia polycrystals. *J Ceram Soc Jpn* 1994;**102**:175.
19. Qian L, Li M, Zhou Z, Yang H, Shi X. Comparison of nano-indentation hardness to micro hardness. *Surf Coat Technol* 2005;**195**:264.
20. Musil J, Kunc F, Zeman H, Polakova H. Relationships between hardness, Young's modulus and elastic recovery in hard nanocomposite coatings. *Surf Coat Technol* 2002;**154**:304.
21. Cheng Y-T, Cheng C-M. What is indentation hardness? *Surf Coat Technol* 2000;**133–134**:417.
22. Fischer-Cripps AC. Critical review of analysis and interpretation of nanoindentation test data. *Surf Coat Technol* 2006;**200**:4153.
23. Sakai M. Energy principle of the indentation-induced inelastic surface deformation and hardness of brittle materials. *Acta Metall Mater* 1993;**41**:1751.
24. Gong J, Wu J, Guan Z. Examination of the indentation size effect in low-load Vickers hardness testing of ceramics. *J Eur Ceram Soc* 1999;**19**:2625.
25. Ren XJ, Hooper RM, Griffiths C, Henshall JL. Indentation size effect in ceramics: correlation with *H*/*E*. *J Mater Sci Lett* 2003;**22**:1105.
26. Morris DJ, Myers SB, Cook RF. Sharp probes of varying acuity: instrumented indentation and fracture behavior. *J Mater Res* 2004;**19**:165.
27. Field JS, Swain MV, Dukino RD. Determination of fracture toughness from the extra penetration produced by indentation-induced pop-in. *J Mater Res* 2003;**18**:1412.
28. Hannink RHJ, Swain MV. Metastability of the martensitic transformation in a 12 mol% ceria–zirconia alloy: 1. Deformation and fracture observations. *J Am Ceram Soc* 1989;**72**:90.
29. Basu B. Toughening of yttria-stabilized tetragonal zirconia ceramics. *Int Mater Rev* 2005;**50**:239.
30. Nowak R, Sekino T, Niihara K. Surface deformation of sapphire crystal. *Phil Mag A* 1996;**74**:171.
31. Bradby JE, Kucheyev SO, Willima JS, Qong-Leung J, Swain MV, Munroe P, Li G, Phillips MR. Indentation-induced damage in GaN epilayers. *Appl Phys Lett* 2002;**80**:383.
32. Kucheyev SO, Bradby JE, Williams JS, Jagadish C, Swain MV. Mechanical deformation of single-crystal ZnO. *Appl Phys Lett* 2002;**80**:956.
33. McElhaney KW, Vlassak JJ, Nix WD. Determination of indenter tip geometry and indentation contact area for depth-sensing indentation experiments. *J Mater Res* 1998;**13**:1300.